Journal of Power Sources 195 (2010) 6997–7002

Contents lists available at ScienceDirect

Journal of Power Sources

journal homepage: www.elsevier.com/locate/jpowsour

Microstructural evolution of ball-milled MgH_2 during a complete dehydrogenation–hydrogenation cycle

Ádám Révész*, Dániel Fátay

Department of Materials Physics, Eötvös University, Budapest, H-1518, P.O.B. 32, Pazmany S 1/A, Budapest, Hungary

ARTICLE INFO

Article history:
Received 16 November 2009
Received in revised form 12 April 2010
Accepted 25 April 2010
Available online 4 May 2010

Keywords:
Sorption
Magnesium
Hydrogen storage
X-ray line profile analysis
Nanocrystal
Grain size

ABSTRACT

Repeated dehydriding–hydriding cycles of ball-milled nanocrystalline MgH_2 was carried out in a Sieverts'-type apparatus. In order to characterize the microstructural changes during a complete $MgH_2 \rightarrow Mg \rightarrow MgH_2$ transformation, the fourth desorption and subsequent absorption were interrupted at different hydrogenation stages. Convolutional multiple whole profile fitting procedure of the corresponding X-ray diffractograms was applied to reveal the evolution of microstructural parameters during the sorption cycle, such as average coherent domain size and crystallite size distribution. Complementary analysis of lattice parameters was also carried out. In this paper we demonstrate that analysing solely the evolution of microstructural parameters during cycling leads to similar rate-controlling mechanisms obtained by sorption kinetic measurements.

1. Introduction

The novel approaches to reach hydrogen based energy systems resulted in a great interest to metal/intermetallic hydride storage solutions. Magnesium is considered as one of the most attractive hydrogen storage materials, mainly because of high storage capacity (7.6 wt.%), lightweight and low cost [1]. Nevertheless, high thermodynamic stability ($\Delta H = -75\,kJ\,mol^{-1}$) [2], high hydrogen desorption temperature (higher than 400 °C) and relatively poor hydrogen absorption–desorption kinetics at temperatures below 350 °C impedes the use of Mg in industrial applications.

It is well known that a breakthrough has been achieved in the magnesium hydride technology by preparing nanocrystalline hydride powders by using high-energy ball milling technique [3–7]. Ball milling of MgH_2 up to several hours results in fine nanopowder with a typical average grain size ranging from 10 to 30 nm [8–12], independently from the type of the milling apparatus and the milling conditions [13]. By reducing the grain size to nanocrystalline dimensions, the H-sorption kinetics are accelerated substantially, and the hydrogen desorption temperature is decreased by about 100 °C [12,14,15]. In recent studies, it was demonstrated that the powder particle size reduction [16] as well as the shape of the particles [17] have also significant effect on the H-sorption kinetics of nanocrystalline Mg/MgH_2 powders.

Numerous studies have been presented on the hydriding–dehydriding reactions of powders in order to model their kinetic properties [18,19]. Calculations based on different rate-controlling mechanisms obtaining density of nucleation sites, H diffusion coefficient, shape of particles, predict the character of the desorption [20]. However, if a size distribution of the transforming grains is taken into account, the shape of the measured curves do not determine unambiguously the rate-controlling mechanism of hydrogen sorption, since the kinetics are strongly affected by the microstructure [21]. From the viewpoint of technological application, it is important to stabilize the kinetics and capacity during several cyclings, which are directly related to the microstructure of the hydriding powder. As reported in a recent paper, the first full dehydrogenation–hydrogenation cycle increase the average crystallite size of ball-milled MgH_2 from 9 to 18 nm and stabilize the microstructure, i.e. repeated cyclings do not have any further significant affect [22].

In the present study, the evolution of the microstructure of ball-milled MgH_2 during one full hydrogen desorption–absorption cycle will be monitored by applying X-ray line profile analysis.

2. Experimental

Commercial polycrystalline MgH_2 powder (supplied by Sigma-Aldrich, purity 99.9%, initial powder particle size 10 μm [12]) was ball-milled in a self-constructed Bakker-type vibratory mill [23] for 10 h under H-atmosphere of 6 atm in order to obtain nanocrystalline material. The milling vial as well as the ball (diameter

* Corresponding author. Tel.: +36 1 372 2823; fax: +36 1 372 2811.
E-mail address: reveszadam@ludens.elte.hu (Á. Révész).

0378-7753/$ – see front matter © 2010 Elsevier B.V. All rights reserved.
doi:10.1016/j.jpowsour.2010.04.085

60 mm) exhibiting vertical vibrations of 50 Hz were made of hardened stainless steel.

Hydrogen sorption kinetics were measured by a Sieverts'-type apparatus (PCT) at 573 K. The ~100 mg sample was loaded into a 10 cm^3 reactor. Desorption was measured in vacuum and absorption under hydrogen pressure of 8 bar. In order to achieve partially desorbed and absorbed states, the desorption (or absorption) process was interrupted in the PCT device at desired intermediate hydrogen content states by quenching the powder to room temperature.

The evolution of the microstructure during desorption-absorption cycles was monitored by X-ray powder diffraction (XRD) with Cu-K_α radiation on a Philips X'pert powder diffractometer in θ–2θ geometry and was characterized by X-ray line profile analysis. The instrumental pattern was measured on a NIST SRM660a LaB_6 peak profile standard material. The lattice parameters of Mg and MgH_2 were determined by a least square fitting algorithm considering the Bragg indices and the corresponding peak positions.

3. X-ray evaluation method

X-ray diffraction peak profile analysis is a powerful method for determining the microstructural properties of ultrafine-grained materials. The effects of crystallite size and lattice strain on peak broadening can be separated on the basis of their different diffraction order dependence. The standard methods of X-ray diffraction profile analysis based on the full width at half-maximum, the integral breadths and on the Fourier coefficients of the profiles provide the apparent crystallite size and the mean square of lattice strains [24–27]. Convolutional Multiple Whole Profile (CMWP) fitting procedure is well-established method for the determination of crystallite size distribution and the lattice defects of materials [28]. By using the appropriate instrumental diffraction pattern, the procedure can be used in a straightforward manner, either when the data are collected with monochromatic or with conventional K_α doublet radiation. In this model it is assumed that the crystallites are spherical and have a lognormal size distribution:

$$G(x) = (2\pi)^{-1/2}\sigma^{-1}x^{-1}\ \exp\left[\frac{-(\ln(x/m))^2}{2\sigma^2}\right], \tag{1}$$

where σ and m are the variance and median of the distribution, respectively. In the CMWP evaluation the whole measured diffraction pattern is fitted directly by the sum of background, theoretically constructed profile functions and measured instrumental profiles. These profile functions are calculated for each reflection as the inverse Fourier transform of the product of the theoretically well-established size and strain Fourier coefficients and the Fourier coefficients of the corresponding measured instrumental profile:

(2)$A(L) = A_L^S(m,\sigma)\,A_L^D(\rho, R_e, \bar{C}, b)\,A_L^I$, where L is the Fourier length, A^S are the size Fourier coefficients, A^D are the strain Fourier coefficients and A^I are the Fourier coefficients of the measured instrumental profile. ρ (average volumetric defect density, mainly dislocations), R_e (effective outer cut-off radius of dislocations), $\bar{C}$ (average dislocation contrast factor [29–30]) and b (Burgers vector) are the strain parameters. The size Fourier coefficients can be expressed as [31]:

$$A_L^S \cong \int_{|L|}^{\infty}(\mu^2 - |L|\mu)\mathrm{erfc}\left\{\left[\frac{\ln(\mu/m)]}{2^{1/2}\sigma}\right]\right\}\mathrm{d}\mu. \tag{3}$$

The background can be determined as a spline going through intensity values defined interactively by the user. The fitting procedure provides both the size and strain parameters, with m and σ the average coherent crystallite size

$$\langle D\rangle = m\exp(2.5\,\sigma^2) \tag{4}$$

can be determined. The CMWP fitting program can be used via its web interface [32].

4. Results

As was demonstrated recently, the change in the sorption behaviour (i.e. rate and maximum capacity) of ball-milled MgH_2 is minor after a couple of hydriding cycles accompanied with constant microstructural parameters corresponding to each fully absorbed state [22], therefore the 4th complete cycle was selected to monitor the microstructural changes within one full desorption-absorption cycle. Fig. 1a and b presents the desorption and absorption curve during the 4th cycle, respectively, obtained by PCT. As seen, the desorption needs about 850 s for completion, while the absorption is completed within 750 s. The observed overall capacity (5.8 wt.%) is somewhat below the theoretical value [1], but comparable with literature data [14,33]. The partially desorbed states corresponding to 10%, 40% and 80% desorbed fraction are denoted by circles in Fig. 1. Since the fully desorbed powder containing only pure Mg is extremely flammable, the 80% fraction was not exceeded for safety reasons. Subsequent absorption was also stopped at different stages, i.e. 15%, 50% and 90% of Mg powder transformed to hydride. It is noted that each partial hydrogenation state was performed on a new dose of the ball-milled material.

A general view on the effect of hydrogen release and absorption during the investigated 4th complete cycle can be inferred

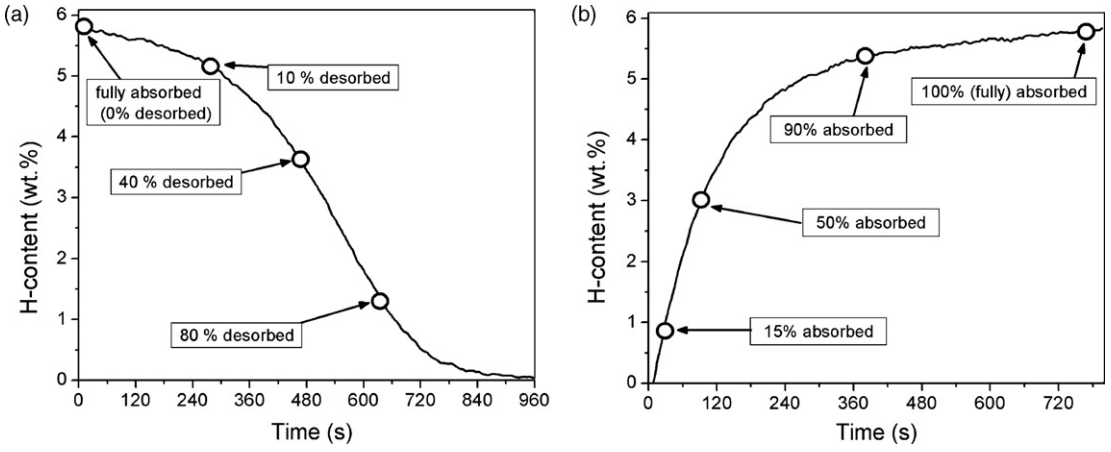

Fig. 1. Fourth desorption (a) and absorption curve (b) of ball-milled nanocrystalline MgH_2. Circles denote partially hydrided states.

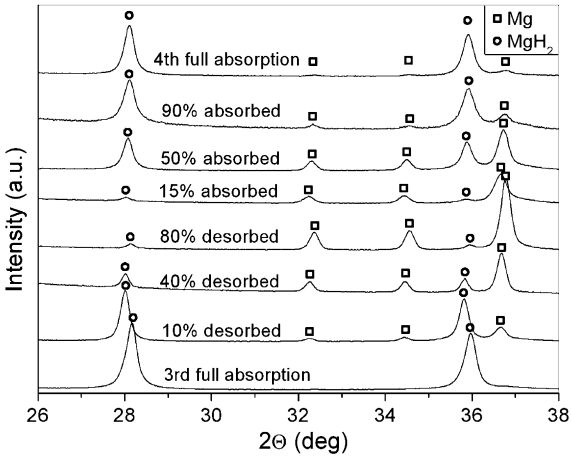

Fig. 2. Series of XRD patterns corresponding to different hydrided states of MgH_2.

from the corresponding X-ray diffractograms (Fig. 2). The fully absorbed state is only characterized by the Bragg-peaks of tetragonal MgH_2 (space group: $P4_2/mnm$ (136), lattice parameters: $a = 4.517$ Å, $c = 3.021$ Å [34]), whilst no trace of γ-MgH_2 is present [35]. Note that the Fe contamination originating from the milling media is negligible according to previous elemental analysis [22]. As the H content decreases continuously, the Bragg-peaks corresponding to hexagonal Mg (space group: $P6_3/mmc$ (194), lattice parameters: $a = 3.209$ Å, $c = 5.211$ Å [36]) evolve gradually. Evidently, the 80% desorbed state is mainly characterized by Mg. As the absorption takes place, the evolution is the opposite, i.e. the Mg peaks almost diminish in line with the development of the tetragonal phase.

A typical example of the fitted pattern by the CMWP method is shown in Fig. 3. The difference plot between the measured and fitted patterns is also given. In the following we will focus on the parameter $\langle D \rangle$ (see Eq. (4)) obtained from the $A_L^S(m,\sigma)$ coefficients, since the variables of the $A_L^D(\rho, R_e, \bar{C}, b)$ function have slight physical information in the case of a tetragonal phase. The obtained values of m and σ are listed in Table 1.

Fig. 4a and b envisages the variation of the crystallite size $\langle D \rangle$ of MgH_2 determined from the CMWP method during desorption and absorption, respectively. As seen, the initial value of $\langle D \rangle = 20$ nm remains practically unchanged up to 40% of desorption; however, as the $MgH_2 \rightarrow Mg$ transformation goes on, the volume fraction of the remaining MgH_2 phase continuously decreases. At the end of the process (80% of desorption) the remaining small amount of MgH_2 forms very small nanoclusters with an average diameter of 3 nm. A considerably different crystallite size evolution takes place during the $Mg \rightarrow MgH_2$ transformation, i.e. $\langle D \rangle$ increases almost linearly up to 19 nm with the total amount of MgH_2. The determination of the average crystallite size of the Mg phase in some states was not adequate due to the small Mg peak intensities. In addition, the obtained lattice defect density (6×10^{13} m^{-2}) leads to an average defect distance, $L = \rho^{-1/2}$, ($L \geq 130$ nm) which considerably exceeds the average crystallite size $\langle D \rangle$ at any absorbed state. Consequently, most of the grain interiors can be considered as defect-free.

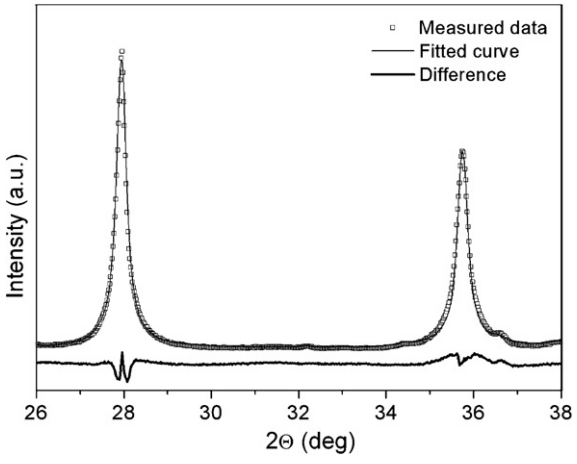

Fig. 3. Measured XRD pattern, function fitted by the CMWP method and difference between the measured and fitted data.

The variation of the lattice parameters of the tetragonal MgH_2 and hexagonal Mg phases during the full sorption cycle exhibits some characteristic features (Fig. 5a and b). Both parameters, a and c of MgH_2 obeys a maximum during the hydrogen release (at 10% of desorption) corresponding to a relative lattice dilatation of about 0.1–0.2%. As the hydrogen is almost fully released from the powder, the parameters of the remaining very few amount of MgH_2 are slightly lower than those of the initial state; however, the error of the data is significantly higher due to the small intensity of the corresponding Bragg-peaks (see Fig. 2). At the first absorption state (15%) a and c parameters exhibit a slight increase. As the absorption continues, both values level off at around 4.515 and 3.025 Å, respectively.

A slightly different behaviour is observed for the hexagonal Mg. The parameters of the negligibly amount of Mg in the fully absorbed state are close to the literature values [36]. Similar to the MgH_2 phase, the c parameter reveals an increase of 0.17% during the hydrogen release; however, the value of the a parameter scatters around 3.215 Å. At the most desorbed state (80% of desorption) dominated mainly by Mg grains, both values reach its minimum indicating a considerable lattice contraction. As the hydrogen absorption begins during the second part of the sorption

Table 1
Values of median (m) and variance (σ) obtained by the CMWP method for different sorption states.

Sorption state	m (nm)	σ
3rd Fully absorbed	8.5	0.57
10% Desorbed	10.9	0.53
40% Desorbed	6.4	0.70
80% Desorbed	0.1	1.27
15% Absorbed	0.3	1.06
50% Absorbed	2.96	0.70
90% Absorbed	6.24	0.62
4th Fully absorbed	8.3	0.58

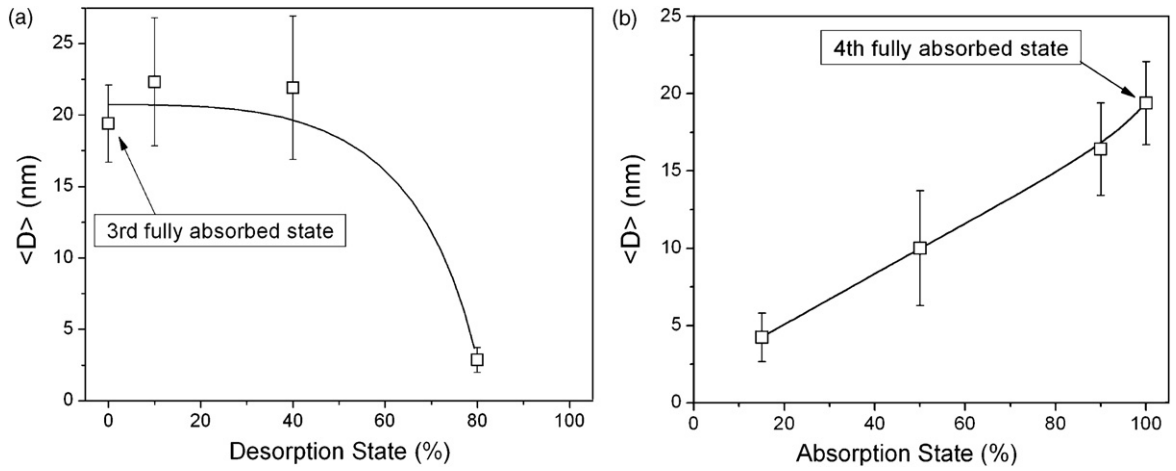

Fig. 4. Variation of average coherent crystallite size of tetragonal MgH_2 during desorption (a) and absorption (b).

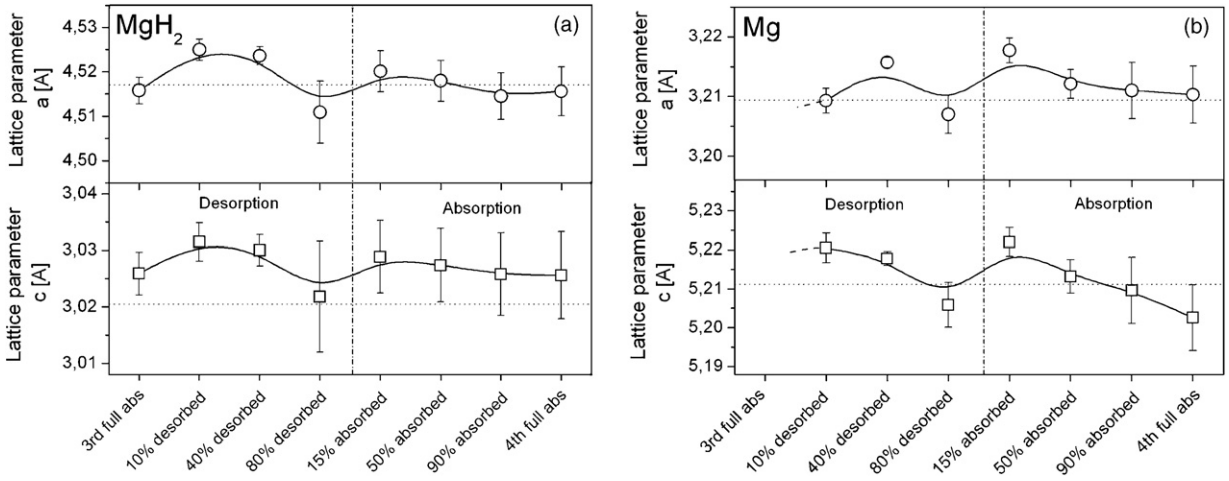

Fig. 5. Variation of lattice parameters of tetragonal MgH_2 (a) and hexagonal Mg (b) during desorption and absorption. Horizontal dotted lines indicate literature values.

cycle, an instantaneous increase in both parameters is observed followed by a slight but considerable decrease up to full hydrogenation. From the variation of the unit cell volume during the complete cycling, the mean square strain is estimated as 0.1–0.3% accumulated mainly at the grain boundaries, since the CMPW method results in a very low volumetric defect density.

5. Discussion

As reported in a recent study, ball milling of commercial MgH_2 results in a relatively inhomogeneous crystallite size distribution with an average grain size of 9 nm [22]. The first desorption-absorption cycle changes the microstructure significantly, the coherent domain size increases from 9 to 18 nm, meanwhile the distribution becomes more homogeneous. At the same time the average powder particle size (~0.8 μm) and its distribution obtained from scanning electron microscopy show almost no change after cycling [37]. The subsequent second cycling destroys the homogeneity on the nanoscale; however, subsequent hydrogenation–dehydrogenation does not change the microstructure considerably, the value of $\langle D \rangle$ of MgH_2 stabilizes at around 20 nm, in accordance with the work of Danaie and Mitlin [8]. Although the 3rd and 4th fully absorbed hydride powders are in similar states, Figs. 4 and 5 imply significant changes occurring in between.

The characteristic differences in the crystallite size evolution during desorption and absorption suggest different kinetic processes. As was presented in Fig. 4a, in spite of the continuously decreasing amount of MgH_2, the value of $\langle D \rangle$ is unchanged (~20 nm) up to 40% hydrogen release. This kind of transformation can be ascribed by instantaneous $MgH_2 \rightarrow Mg$ conversion of randomly selected particles, which does not influence the average crystallite size of the remaining hydride phase. It is well known if the nucleation (and growth) of the new phase begin randomly in the bulk, the transformation can be described by the classical Johnson–Mehl–Avrami (JMA) model [38,39]. This type of transformation was also confirmed by fitting a total reacted function of a multi-particle MgH_2 system on the measured hydrogen desorption curves [21]. According to the thermodynamic model for hydrogenation of metals, in which a coherency strain generated by the transforming phase (metal ↔ hydride), a macroscopic thermodynamic barrier evolves [40]. This barrier opposes a continuous hydriding–dehydriding transformation inside a grain. On contrary, an abrupt conversion of a metal grain into a hydride one's takes place, i.e. at a certain H pressure the powder agglomerate contains fully transformed and untransformed grains. The dominance of the remaining extremely small hydride nanoparticles (~3 nm) at the end of the desorption process can only be explained by the JMA theory, if additional considerations on the microstructure are taken into account. Since this crystallite size is below the critical Hall-Petch length [41], these particles are free of lattice defects (in accordance with the results obtained from the CMWP analysis), which act as preferred nucleation sites in a JMA process. As a consequence, the small grains are activated and transform to Mg ultimately.

As presented in Fig. 4b, $\langle D \rangle$ of MgH_2 increases proportionally with the H content up to 19 nm during the absorption. The increasing hydride size assumes a transformation where the hydrogen atoms are initially bonded at the surface and then the converted fraction continuously evolves into the bulk. In the literature, this kind of transformation is labelled as the contracting volume model (CV) [38,42]. The main assumption of this model is that the initial nucleation on the surface is fast compared to the overall growth kinetics and the nucleation zone is thin compared to the particle diameter [19]. In accordance, the kinetic analysis of the PCT absorption curves of a magnesium powder agglomerate confirms the CV mode of transformation [21].

The observed characteristic features of tetragonal MgH_2 and hexagonal Mg lattice parameters (see Fig. 5a and b) can have two different origins, i.e. internal stress and hydrogen in solid solution can both alter the average bond length. The large difference in the unit cell volume of MgH_2 (61.638 Å^3) and Mg (45.977 Å^3) can be accountant for a hydrostatic stress accumulation in the powder particles during the $MgH_2 \rightarrow Mg \rightarrow MgH_2$ cycling. Besides, the difference in the lattice parameters at the Mg–MgH_2 interfaces promotes the formation of stress induced lattice defects which offer a path for accelerated hydrogen diffusion.

As was revealed, the increased value of a and c parameters of MgH_2 refer to a dilated structure at an intermediate stage of desorption (see Fig. 5a). During the JMA type of dehydrogenation the transformed particles undergo a volume decrease, resulting in a slight dilation of the neighbouring unreacted hydride particles. The smallest lattice parameters of the 80% desorbed sample (characterized by very few amount of MgH_2 with an average crystallite size of 3 nm) are the consequence of the increased specific surface tension. The almost constant values of a and c during the absorption is in accordance with the practically zero solubility of hydrogen in MgH_2 [43]. In addition, the thickening hydride shell during the CV transformation is not affected by any stress accumulation.

The solid solubility of hydrogen in hexagonal magnesium is about 2 at.% [43]. If hydrogen atoms occupy the energetically favourable tetrahedral interstitial sites, a lattice dilatation takes place [44]. At higher concentrations of hydrogen, the lattice converts to a tetragonal structure in which two tetrahedral and two octahedral interstitial sites are occupied resulting in the MgH_2 phase. Similarly to MgH_2, the lattice parameters of the Mg grains corresponding to the 80% desorbed state exhibit a local minimum reaching the literature values (see Fig. 5b), which refer to lack of stress. At this point the Mg powder is also free of dissolved hydrogen.

At the beginning of absorption (15%) the hexagonal Mg lattice is capable to dissolve enough hydrogen resulting in substantial increase of both lattice parameters (see Fig. 5b). As the transformation goes on, the hydrogen concentration reaches a critical value forming an Mg–MgH_2 interface layer moving continuously from the surface of the grains to the bulk. As also seen, the c parameter corresponding to the decreasing amount of Mg decreases progressively until the fully absorbed state is reached. Those Mg particles which still exist in the fully absorbed state are separated from the hydrogen probably due to some intact oxide layer. This very small fraction of Mg is consequently free of dissolved hydrogen at any state, exhibiting the similar values of lattice parameter as those of the desorbed state.

6. Conclusions

Convolutional multiple whole profile fitting procedure was applied to follow the evolution of the average crystallite size of tetragonal MgH_2 during a complete sorption cycle. It was obtained that the initial value of the MgH_2 grain size remains practically unchanged (20 nm) up to 40% of desorption; however, at the final stage of the $MgH_2 \rightarrow Mg$ transformation the remaining small amount of MgH_2 forms very small nanoclusters with an average diameter of 3 nm. This kind of transformation can be ascribed by instantaneous $MgH_2 \rightarrow Mg$ conversion of randomly selected particles which is the main characteristics of classical JMA model. On contrary, a different crystallite size evolution takes place during the $Mg \rightarrow MgH_2$ transformation, i.e. $\langle D \rangle$ increases almost linearly up to 19 nm. The increasing hydride size assumes a CV-type of transformation. The observed characteristic features of tetragonal MgH_2 and hexagonal Mg lattice parameters can have two different origins, i.e. internal stresses and solute hydrogen.

Acknowledgements

Á.R. is indebted for the János Bolyai Research Scholarship of the Hungarian Academy of Sciences. The assistance of Dr. G. Ribárik in the X-ray line profile analysis is greatly acknowledged. D.F. kindly thanks the possibility of using the PCT device to Prof. T. Spassov.

References

[1] R.C. Bowman, B. Fultz, Materials Research Bulletin 27 (9) (2002) 688–693.
[2] K.H.J. Buschow, P.C.P. Bouten, A.R. Miedema, Report on Progress in Physics 46 (9) (1982) 937–1039.
[3] R.A. Varin, T. Czujko, Ch. Chiu, Z. Wronski, Journal of Alloys and Compounds 424 (1/2) (2006) 356–364.
[4] L. Zaluski, A. Zaluska, P. Tessier, J.O. Ström-Olsen, R. Schulz, Materials Science Forum 225 (1996) 853–858.
[5] G. Liang, S. Boily, J. Huot, A. Van Neste, R. Schulz, Journal of Alloys and Compounds 276 (1/2) (1998) 302–306.
[6] G. Liang, S. Boily, J. Huot, A. Van Neste, R. Schulz, Journal of Alloys and Compounds 268 (1/2) (1998) 302–307.
[7] G. Liang, Journal of Alloys and Compounds 370 (1/2) (2004) 123–128.
[8] M. Danaie, D. Mitlin, Journal of Alloys and Compounds 476 (1/2) (2008) 590–598.
[9] M. Porcu, A.K. Petford-Long, J.M. Sykes, Journal of Alloys and Compounds 453 (1/2) (2008) 341–346.
[10] V. Fuster, G. Urretavizcaya, F.J. Castro, Journal of Alloys and Compounds 481 (1/2) (2009) 673–680.
[11] S. Doppiu, L. Schultz, O. Gutfleisch, Journal of Alloys and Compounds 427 (1/2) (2007) 204–208.
[12] D. Fátay, Á. Révész, T. Spassov, Journal of Alloys and Compounds 399 (1/2) (2005) 237–241.
[13] M. Polanski, J. Bystrzycki, T. Plocinski, International Journal of Hydrogen Energy 33 (7) (2008) 1859–1867.
[14] W. Oelerich, T. Klassen, R. Bormann, Journal of Alloys and Compounds 315 (1/2) (2001) 237–242.
[15] G. Barkhordarian, T. Klassen, R. Borman, Journal of Alloys and Compounds 364 (1/2) (2004) 242–246.
[16] Á. Révész, D. Fátay, D. Zander, T. Spassov, Journal of Metastable and Nanocrystalline Materials 24/25 (2005) 447–450.
[17] K.J. Jeon, A. Theodore, C.Y. Wu, Journal of Power Sources 183 (2) (2008) 693–700.
[18] M.H. Mintz, Y. Zeiri, Journal of Alloys and Compounds 216 (2) (1994) 159–175.
[19] K.C. Chou, Q. Li, Q. Lin, L.J. Jiang, K.D. Xu, International Journal of Hydrogen Energy 30 (3) (2005) 301–309.
[20] G. Barkhordarian, T. Klassen, R. Bormann, Journal of Alloys and Compounds 407 (1/2) (2006) 249–255.
[21] Á. Révész, D. Fátay, T. Spassov, Journal of Materials Research 22 (11) (2007) 3144–3150.
[22] D. Fátay, T. Spassov, P. Delchev, G. Ribárik, Á. Révész, International Journal of Hydrogen Energy 32 (14) (2007) 2914–2919.
[23] C. Suryanarayana, Mechanical Alloying and Milling, Marcel Dekker, New York, 2004.
[24] G.K. Williamson, W.H. Hall, Acta Metallurgica 1 (1) (1953) 22–31.
[25] B.E. Warren, B.L. Averbach, Journal of Applied Physics 21 (6) (1950) 595–599.
[26] J.G.M. van Berkum, A.C. Vermuelen, R. Delhez, T.H. de Keijser, E.J. Mittemeijer, Journal of Applied Crystallography 27 (3) (1994) 345–357.
[27] T. Ungár, A. Borbély, Applied Physics Letters 69 (21) (1996) 3173–3175.
[28] G. Ribárik, J. Gubicza, T. Ungár, Materials Science and Engineering: A 387–389 (2004) 343–347.
[29] T. Ungár, I. Dragomir, Á. Révész, A. Borbély, Journal of Applied Crystallography 32 (5) (1999) 992–1002.
[30] T. Ungár, G. Tichy, Physica Status Solidii A 171 (2) (1999) 425–434.
[31] T. Ungár, J. Gubicza, G. Ribárik, A. Borbély, Journal of Applied Crystallography 34 (3) (2001) 298–310.
[32] http://www.renyi.hu/cmwp.

[33] Z. Dehouche, T. Klassen, W. Oelerich, J. Goyette, T.K. Bose, R. Schulz, Journal of Alloys and Compounds 347 (1/2) (2002) 319–323.
[34] JCPDS card 12-0697.
[35] S. Gialanella, R. Ceccato, F. Casari, G. Ischia, A. Molinari, CALPHAD 33 (1) (2009) 82–88.
[36] JCPDS card 35-0821.
[37] Á. Révész, D. Fátay, T. Spassov, Journal of Alloys and Compounds 434/435 (2007) 725–728.
[38] P.W.M. Jacobs, F.C. Tompkins, in: W.E. Garner (Ed.), Chemistry of the Solid State, Butterworth, London, 1955, pp. 184–212.
[39] M. Avrami, Journal of Chemical Physics 8 (1940) 212–223.
[40] R.B. Schwarz, A.G. Khachaturyan, Acta Materialia 54 (2) (2006) 313–323.
[41] E.O. Hall, Yield Point Phenomena in Metals and Alloys, Plenum Press, New York, 1970.
[42] L.E. Gabis, A.P. Voit, E.A. Evard, Y.V. Zaika, L.A. Chernov, V.A. Yartys, Journal of Alloys and Compounds 404–406 (2005) 312–316.
[43] Z.D. Popovic, G.R. Piercy, Metallurgical and Materials Transactions A 6 (10) (1975) 1915–1917.
[44] N. Novakovic, L. Matovic, J.G. Novakovic, M. Manasijevic, N. Ivanovic, Materials Science and Engineering B (2009), doi:10.1016/j.mseb.2009.06.15.